RSC Advances




ROYAL SOCIETY OF CHEMISTRY

www.rsc.org/advances

# The in situ small-angle X-ray scattering study of structural effects of temperature and draw ratio of hot-drawing process on ultra-high molecular weight polyethylene fibers

**Minfang An[a], Haojun Xu[a], You Lv[a], Qun Gu[b], Feng Tian[c] and Zongbao Wang[a*]**

**[a] Ningbo Key Laboratory of Specialty Polymers, Faculty of Materials Science and Chemical Engineering, Ningbo University, Ningbo 315211, China**

**[b] College of Material Engineering, Ningbo University of Technology, Ningbo 315211, China**

**[c] Shanghai Institute of Applied Physics, Chinese Academy of Sciences, Shanghai 201204, China**

*** Corresponding author. E-mail address: wangzongbao@nbu.edu.cn.**

**Abstract**

The in situ small-angle X-ray scattering (SAXS) study of structural effects of temperature and drawing ratio ($DR_1$) of hot-drawing process on Ultra-high molecular weight polyethylene (UHMWPE) gel fibers was performed with the equipment of simulating the hot-drawing process in industrial product line. The UHMWPE gel fibers were prepared from the industrial production line. The results show that the increase of hot-drawing temperature has significant effect on the kebab but no obvious effect on shish length and misorientation. The increase of temperature is beneficial to the formation of shish at suitable temperature range of 124-130 °C, while the formation

of shish at high temperature 140 °C needs higher $DR_1$. Moreover, the increase of $DR_1$ is good to the formation of shish at all experimental hot-drawing temperatures, while the kebab formation mainly occurs at low $DR_1$ and the kebab transformation mainly happen at high $DR_1$. The shish length and misorientation decreases with the increase of $DR_1$.

*Keywords:* Ultra-high molecular weight polyethylene fibers, in situ small-angle X-ray scattering, shish-kebab, hot-drawing

## 1 Introduction

Ultra-high molecular weight polyethylene fibers (UHMWPE) are typical high-performance fibers produced by gel spinning method from flexible polymer chains, which have been wildly applied in high-tech fields such as aerospace, national defense and military, safety protection due to its excellent performance such as low density, high specific strength and modulus, excellent energy absorption[1-7]. The high orientation and crystallinity of the molecular structure endows UHMWPE fibers with excellent mechanical properties. However, the highest tensile strengths and moduli achieved for UHMWPE fibers are still far below those of theoretical[8]. Therefore, to further improve the mechanical performance, a lot of investigations on the structural evolution of UHMWPE fibers have been done. Pennings et al.[9] found that the UHMWPE fibers with the draw ratio of 6 were composed of shish-kebabs, while fully drawn fibers with the draw ratio of 80 consisted of extended chain crystal.

Hoogsteen et al.[10] investigated hot-drawing process of UHMWPE gel fibers through wide-angle x-ray scattering (WAXS) and small-angle x-ray scattering (SAXS). They found that fibers with low hot-drawing ratio contained originally lamellar or shish-kebab structure and those with high hot-drawing ratio contained almost fibrils transformed from the kebab crystal. Ohta et al.[11] discovered that the UHMWPE fibers had heterogeneous cross-sectional morphology as the skin-core structure at a relatively low spinning speed possesses. The skin was composed of an interlocked shish-kebab structure, while the core was composed of a lamella-stacking structure. Moreover, they found that the fibers obtained at relatively high spinning speed process were composed of homogeneous alignment of the shish-kebab crystals and exhibited better drawability and corresponding better tensile properties. Yeh et al.[12] studied the influence of draw ratios on the structure of gel-spinning UHMWPE fibers, and found that the chain-folded molecules in kebab crystals of the as-prepared UHMWPE fiber specimens gradually transformed into shish-like crystals with relatively high orientation as their draw ratios value increased from 1 to 20, while only shish crystals were observed on the surfaces of drawn UHMWPE fiber specimens with draw ratios values higher than 20. Litvinov et al.[13] researched the final drawing stage of UHMWPE fibers, and found the structure of fibers gradually transformed into extended chain crystal with the draw ratio value increasing. In addition, many other previous studies[14-16] were done for the structural evolution of UHMWPE fibers. From the above results, the key point of obtaining higher performance UHMWPE fibers is to make fibers with a higher draw ratio during

spinning process, and consequently more molecules can be involved in the formation of extended chain crystals. More extended chain crystals content in UHMWPE fibers makes higher degree of orientation and crystallinity, and hence better performance[17]. But the influence of the formation and evolution of shish-kebab structure on mechanical performance of UHMWPE fibers was still not clear. Moreover, the spinning solution concentration used in most above studies was much lower than the practical industrial concentration, which made the research results can not reflect the actual situation of structural evolution of shish-kebab crystal at different draw ratio and temperature in practical industrial production line.

In order to better investigate the actual structural evolution mechanism of UHMWPE fibers, Tian et al.[18-19] investigated the formation and transition of shish-kebab crystal of UHMWPE fibers during ultra-high hot stretching at varying temperature of 80, 90 and 100 °C via in situ small and wide angle X-ray scattering. They believed that the formation of shish structure accompanied by the break-reorganization of original lamellae at low temperature of 80 °C, while shish-kebab structure smoothly transformed to shish structure with no significant break of kebab crystal at 100 °C. But the temperature of hot stretching was much lower than that in practical industrial production line. Moreover, the hot-stretching process, which was adopted by Tian et al. to research the structural evolution of UHMWPE fibers, is very different with the hot-drawing process of practical industrial production line. So these studies can not really reflect the structural evolution of shish-kebab of UHMWPE fibers at different draw ratio and temperature in practical

industrial production line.

Small-angle X-ray scattering (SAXS) is the very effective method for the research of the microstructure of polymer materials. Moreover, its theory has been fully developed that can be applied for the measurement of polymer lamellae, polymer microfibrils and microvoids[20-22]. Furthermore, with the awareness of the value of synchrotron radiation and continuous development, the in situ X-ray measurements have become available and popular for the various studies[23].

In this study, the actual structural effects of temperature and draw ratio on UHMWPE fibers in industrial production line were studied by in situ SAXS. The equipment of simulating the hot-drawing process of industrial production line was installed on the experiment table for in situ SAXS experiment. The UHMWPE fibers sample was gel fibers, which was prepared from the industrial production line.

## 2 Experimental

### 2.1 Materials

The UHMWPE resin used in this study is associated with a viscosity-average molecular weight ($\bar{M}_V$) of $3.5 \times 10^6$, which was supplied by Sinopec Beijing Yanshan Company.

### 2.2 Sample Preparation

The UHMWPE gels were prepared by twin-screw extruder at 150-250 °C with 8 wt% UHMWPE solutions in paraffin oil. The hot homogenized gels were then gel-spinning

using spinneret plate with 240 conical dies with an exit diameter of 1 mm at an extrusion rate of 8 m/min and an extrusion temperature of 268 °C. After spinning from the spinneret, the fibers were gone through the cold drawing process with drawing ratios ($DR_0$) of 4.19 at room temperature. The gel-spinning fibers were then extracted in a dichloromethane bath to remove paraffin oil. After drying stage, the sample of gel fibers was obtained.

2.3 Hot-drawing test

The equipment of simulating the hot-drawing process of industrial production line was used to perform the hot-drawing process of fibers as in industrial production line, as shown in Fig. 1. The hot-drawing test was performed at varying temperature of 124, 127.5, 130, and 140 °C and different hot-draw ratio ($DR_1$) as shown in Table 1. The different $DR_1$ was obtained by changing the outlet roller speed $s_2$, while the inlet roller speed $s_1$ ($s_1$=0.183 m/min) was remained unchanged. The fiber samples were symmetrically drawn to ensure the conditions of detecting position unchanged. The mechanical data and X-ray data were collected simultaneously during hot-drawing. Moreover, the X-ray data was collected from the X-ray windows as shown in Fig. 1. And the structural information, which was reflected from the X-ray data, was not the structural information of the fibers through the whole hot-drawing process. So the collected X-ray data reflected the information of structure during hot-drawing process.

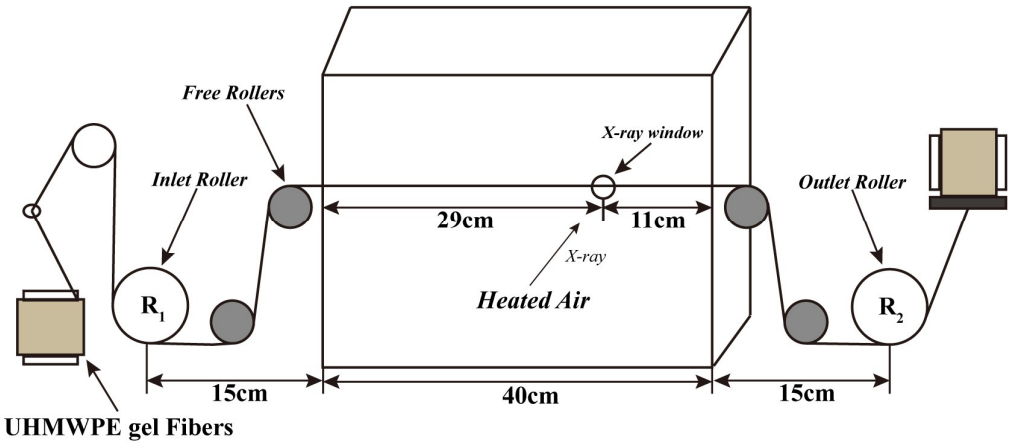


**Fig. 1** The schematic diagrams of in situ SAXS hot-drawing process of UHMWPE gel fibers.

2.4 In situ SAXS measurement

In situ small-angle X-ray scattering (SAXS) measurements were carried out at the BL16B1 beamline in Shanghai Synchrotron Radiation Facility (SSRF). The wavelength of X-ray radiation was 0.124 nm (SAXS). Two-dimensional (2D) SAXS patterns were collected by using a Mar CCD X-ray detector (MAR165) having a resolution of 2048×2048 pixels. The beam intensity monitor before sample was a $N_2$ gas ionization chamber, and the monitor after sample adsorption was a photodiode in the beam stop. Two scatter-less slits (Xenocs) were used to depress parasitic scattering. The sample holder was mounted onto an optical table[24]. The sample-to-detector distance was 5270 mm for SAXS. The SAXS image acquisition time of each data frame was 10 s. All X-ray images were corrected for background scattering, air scattering, and beam fluctuations. The SAXS measurement data analysis was carried out by the Fit2d software package[25].

**Table 1**

The drawing condition of UHMWPE gel fibers in one-step hot-drawing process.

| Sample | $S_1$ (m/min) | $S_2$ (m/min) | Drawing Temperature (°C) | $DR_1$ |
|---|---|---|---|---|
| A1 | 0.183 | 0.366 | 124 | 2 |
| A2 | 0.183 | 0.549 | 124 | 3 |
| A3 | 0.183 | 0.732 | 124 | 4 |
| A4 | 0.183 | 0.915 | 124 | 5 |
| A5 | 0.183 | 1.098 | 124 | 6 |
| B1 | 0.183 | 0.366 | 127.5 | 2 |
| B2 | 0.183 | 0.549 | 127.5 | 3 |
| B3 | 0.183 | 0.732 | 127.5 | 4 |
| B4 | 0.183 | 0.915 | 127.5 | 5 |
| B5 | 0.183 | 1.098 | 127.5 | 6 |
| C1 | 0.183 | 0.366 | 130 | 2 |
| C2 | 0.183 | 0.549 | 130 | 3 |
| C3 | 0.183 | 0.732 | 130 | 4 |
| C4 | 0.183 | 0.915 | 130 | 5 |
| C5 | 0.183 | 1.098 | 130 | 6 |
| C6 | 0.183 | 1.281 | 130 | 7 |
| D1 | 0.183 | 0.366 | 140 | 2 |
| D2 | 0.183 | 0.549 | 140 | 3 |
| D3 | 0.183 | 0.732 | 140 | 4 |
| D4 | 0.183 | 0.915 | 140 | 5 |

| | | | | |
|---|---|---|---|---|
| D5 | 0.183 | 1.098 | 140 | 6 |
| D6 | 0.183 | 1.281 | 140 | 7 |
| D7 | 0.183 | 1.464 | 140 | 8 |
| D8 | 0.183 | 1.647 | 140 | 9 |
| D9 | 0.183 | 1.830 | 140 | 10 |

2.5 Scanning electron microscopy (SEM)

The surface morphologies of UHMWPE gel fibers and drawn fibers were observed by SEM (SU70). The UHMWPE drawn fibers were obtained from the industrial production line, which were gone through the first hot-drawing stage with 4.0 draw ratio at 130 °C. The surface of UHMWPE gel fibers and drawn fibers were respectively treated with hot n-octane at 105-110 °C and 110-115 °C. The samples were sputtered with gold before SEM observation.

**3. Results and discussion**

The 2D SAXS patterns of UHMWPE gel fibers at different temperature and hot-drawing ratio ($DR_1$) are shown in Fig. 2. The scattering vectors along and perpendicular to the fiber axis direction are defined as $q_1$ and $q_2$, respectively ($q = 4\pi \sin\theta/\lambda$, where $2\theta$ is the scattering angle and $\lambda$ is the X-ray wavelength). The isotropic SAXS pattern of UHMWPE gel fiber without hot-drawing at room temperature is shown in the top right corner of Fig. 2, which is caused by the randomly oriented lamellae. The SEM images of UHMWPE gel fibers and first

hot-drawing stage drawn fibers are shown in Fig. 3. The randomly oriented lamellae could be observed obviously in Fig. 3 (a, b), which corresponds to the isotropic SAXS pattern of UHMWPE gel fiber (Fig. 2). In addition, the shish-kebab structure could be clearly observed in Fig. 3 (c, d). The maximum $DR_1$ of UHMWPE gel fibers at 124, 127.5, 130 and 140 °C are 6, 6, 7, and 10, respectively, as shown in Fig. 2. It indicates that the maximum $DR_1$ of gel fibers is increased with the increase of hot-drawing temperature. Moreover, the equatorial scattering patterns along $q_1$ direction, which indicates that the oriented lamellar structure (kebab) becomes stronger with the increase of temperature at the same $DR_1$. Besides, the meridional streaks across the beam stop become more obvious with the increase of $DR_1$ at the same temperature, which indicates the shish crystal structure. In order to further investigate the intensity change of kebab and shish scattering patterns at different temperature and $DR_1$, the scattering intensities from shish and kebabs were integrated from Fig.2 by using the following equations[26]:

$$I_{shish} = \int_{0.03}^{0.3} \int_{70^{\circ}}^{110^{\circ}} I(q, \emptyset)\, dq d\emptyset \qquad (1)$$

$$I_{kebab} = \int_{0.1}^{0.5} \int_{-70^{\circ}}^{70^{\circ}} I(q, \emptyset)\, dq d\emptyset \qquad (2)$$

Where $q$ is the scattering vector and $\emptyset$ is the azimuthal angle.

The shish scattering intensity at different temperature and $DR_1$ are shown in Fig. 4

(a). The value of shish scattering intensity is increased with the increase of $DR_1$, which corresponds to the result of 2D SAXS patterns as shown in Fig. 2. It means that the increase of $DR_1$ is good to the formation of shish. Moreover, the value of shish scattering intensity increases with the increase of temperature when the temperature is below 140 °C. And the shish scattering intensity at 140 °C is obviously lower than that of other three temperatures at the same $DR_1$. But when $DR_1$ is higher than 6, the shish scattering intensity at 140 °C becomes strong. Besides, the gel fibers can obtain higher maximum $DR_1$ at 140 °C than that at other three temperatures. It can be seen from that the high temperature of 140 °C is not good for the formation of shish at low $DR_1$, while the high $DR_1$ is conducive to the formation of shish. These results indicate that the increase of temperature is beneficial to the formation of shish at suitable temperature range, while the formation of shish at high temperature such as 140 °C needs higher $DR_1$.

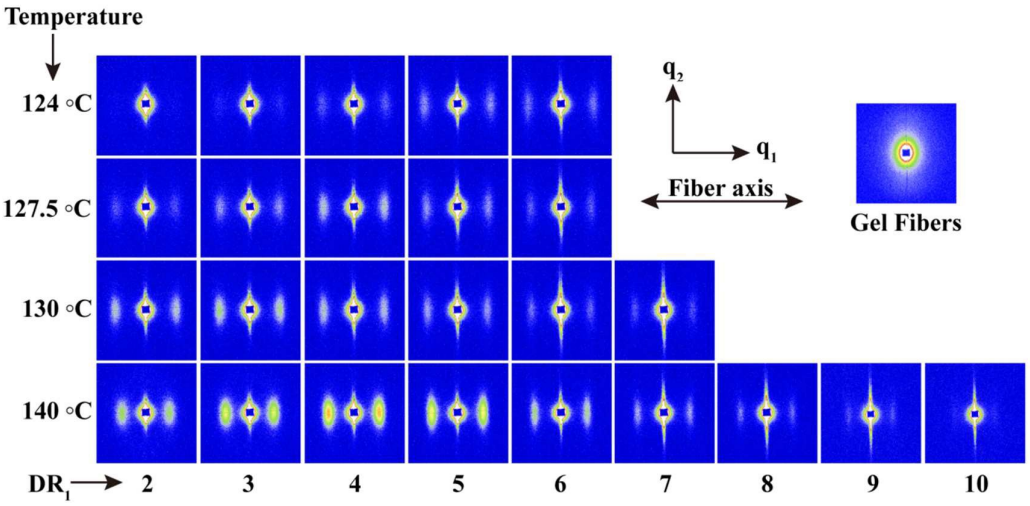


**Fig. 2** The 2D SAXS patterns of UHMWPE gel fibers at different temperature and hot-drawing ratio

($DR_1$) and the UHMWPE gel fibers without hot-drawing at room temperature.

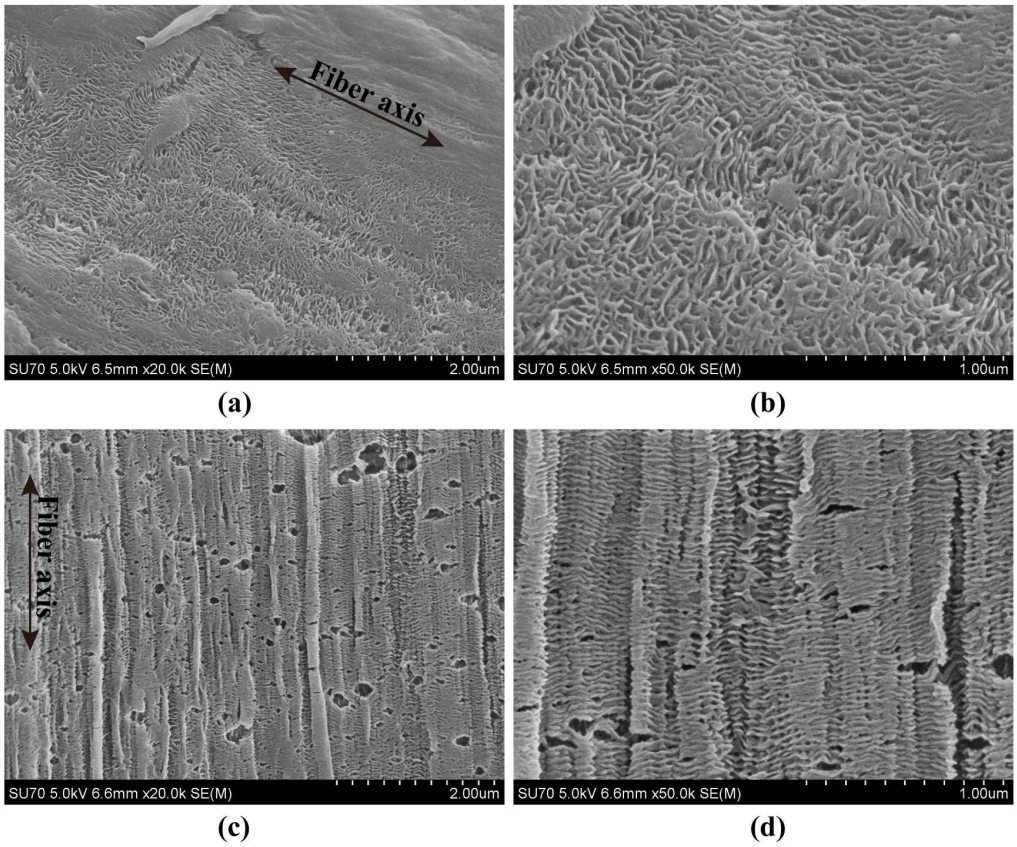


**Fig. 3** SEM images of UHMWPE gel fibers and drawn fibers: (a, b) the gel fibers, (c, d) the drawn fibers at first hot-drawing stage.

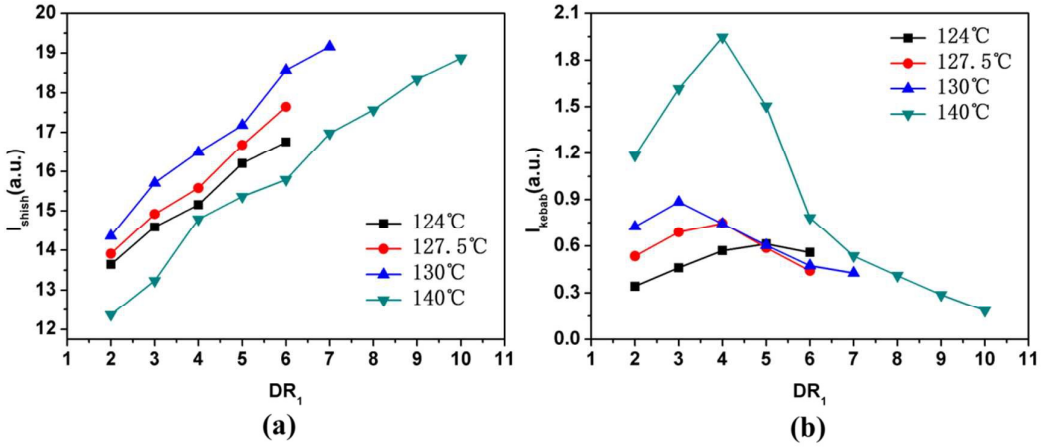

**Fig. 4** The scattering intensities from shish and kebabs at different temperature and $DR_1$: (a) the scattering intensity of shish, (b) the scattering intensity of kebab.

Fig. 4 (b) shows the kebab scattering intensity at different temperature and $DR_1$. The kebab scattering intensity firstly increases and then decreases with the increase of $DR_1$. The increase of kebab scattering intensity indicates the formation of kebab (lamellae), while the decrease of kebab scattering intensity means the transformation of kebab to shish. The $DR_1$ of the highest kebab scattering intensity is the transition point of formation and transformation of kebab. When the $DR_1$ is lower than the transition point, the formation of kebab is predominant process in hot-drawing process. In other words, the main process is the transformation of kebab when the $DR_1$ is higher than the transition point. The $DR_1$ of the highest kebab scattering intensity at temperature of 124, 127.5, 130 and 140 $^{\circ}$C are 5, 4, 3, and 4, respectively. It can be seen that the transition point moves to the lower $DR_1$ with the increase of temperature when the temperature is lower than 140 $^{\circ}$C. This result implies that the increase of temperature is conducive to the transformation of kebab to shish when the temperature is lower than 140 $^{\circ}$C, which corresponds to the result of the shish scattering intensity. The reason is that the transformation of kebab to shish is the melting recrystallization process in stretching field in the experimental conditions of this study, which makes the increase of temperature good to the transformation of kebab. Moreover, at relatively low $DR_1$, high temperature is conducive to the formation of shish and kebab, so the scattering intensity of shish

and kebab are both improved with the increase of temperature. At relatively high $DR_1$, the molecular chain, which could take part in crystal, all have been crystallized. So the increase of shish scattering intensity corresponds to the decrease of kebab scattering intensity, i.e., higher shish scattering intensity accompanies the lower kebab scattering intensity. As a consequence, the transition point moves to the lower $DR_1$ with the increase of temperature when the temperature is lower than 140 °C. And the temperature has significant influence on the both formation and transformation of kebab at 140 °C due to the fact that the temperature of 140 °C is very close to the melt temperature of UHMWPE fibers, which makes the kebab more thickness form at 140 °C. So the transition point is at 4 $DR_1$, which is not too lower or not too high comparing with temperature that lower than 140 °C. In addition, the kebab scattering intensity at 140 °C is much higher than other three temperatures when $DR_1$ is lower than 6. It means that the kebab which was formed at 140 °C is much larger than that at other three temperatures and difficultly transformed to shish. This is why the shish scattering intensity at 140 °C is lower than other temperatures at the same $DR_1$. But the kebab scattering intensity at 140 °C decreases with the increase of $DR_1$ when $DR_1$ is higher than 4. It indicates that the transformation of kebab at high temperature such as 140 °C needs higher $DR_1$, which corresponds to the formation of shish at 140 °C. Moreover, it should be noted that the kebab scattering intensity is lower than the actual scattering intensity of kebab at relative high $DR_1$ due to the fact that fibers became thinner with the increase of $DR_1$. Therefore the transition point mentioned above is slightly lower than the actual

value.

To further study the structural effects of temperature and drawing ratio of hot-drawing process on UHMWPE fibers in industrial product line, more parameters about shish and kebab structure were calculated from the SAXS patterns. Two parameters to describe the kebab structure, namely the long period $L$ and the lateral dimension of the kebab, are derived from the SAXS data measured along the meridian. The long spacing of stacks of kebab along the fiber axis direction can be obtained by considering the scattering intensity distribution along the $q_1$ direction $I(q_1)$, which was obtained by meridian scans along $q_1$ for certain intervals of $q_2$ as schematically shown in Fig. 2 and Fig. 5(a). And the long period of the samples, $L$ measured along $q_1$, was calculated from the peak position of $I(q_1)$ according to Bragg's law:

$$L = 2\pi/q_{1,max} \qquad (3)$$

The $\Delta q_1$, which is shown in Fig. 5(a), is the width of peaks at half height of $I(q_1)$ curves, which represents the distributions of long period, $L$. In order to obtain the accurate peak position of $I(q_1)$ and $\Delta q_1$, the one-dimensional SAXS curves were fitted by Lorentz as shown in Fig. 5(a).

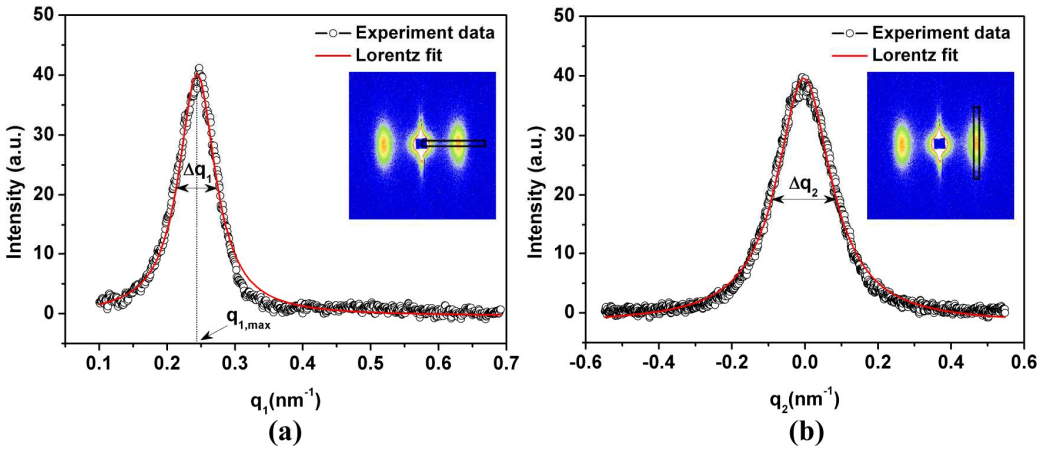


**Fig. 5** (a) Fitting process of long period, (b) fitting process of lateral size of kebab crystals.

The lateral size of kebab structure $L_{SAXS}$ can be derived from the width $\Delta q_2$ of the peaks at half height in the equatorial direction according to the following equation[27]:

$$L_{SAXS} = 2\pi/\Delta q_2 \qquad (4)$$

The $\Delta q_2$ was obtained by Lorentz fitting, which is shown in Fig. 5(b).

The average shish length, $\langle L_{shish} \rangle$, and the misorientation of shish, $B_{\emptyset}$, were obtained by using the Ruland streak method to analyze the meridional streak feature in SAXS[28-30]. Ruland demonstrated that the size and orientation distributions of longitudinal voids in polymer and carbon fibers in real space could be estimated from the meridional streak of SAXS in reciprocal space (as long as the orientation and the longitudinal length of scatterer are finite). Since the method is principally based on the separation of experimentally measured azimuthal breadth from contributions of

scatterer length and misorientation, the method can also be applied to separate the average length of shish and its average misorientation. If one assumes that all azimuthal distributions can be modeled by Lorentz functions, the observed azimuthal width, Bobs, can be related to the length of shish, $\langle L_{shish} \rangle$, and the azimuthal width, $B_{\emptyset}$, due to misorientation of shish by the following equation.

$$B_{obs} = \frac{1}{\langle L_{shish} \rangle s} + B_{\emptyset} \quad (5)$$

If all azimuthal distributions have Gaussian expressions, then the relationship becomes

$$B_{obs}{}^2 = \left(\frac{1}{\langle L_{shish} \rangle s}\right)^2 + B_{\emptyset}{}^2 \quad (6)$$

where $B_{obs}$ represents the integral width of the azimuthal profile from the meridional streak at $s$ ($s$ is the scattering vector, where $s = q/2\pi = 2\sin\theta/\lambda$). On the basis of equation (5) or equation (6), $\langle L_{shish} \rangle$ can be obtained from the slope, and the misorientation width, $B_{\emptyset}$ can be obtained from the intercept of the plots ($B_{obs}$ vs $s^{-1}$ or $B_{obs}^2$ vs $s^{-2}$). In this study, we found that all azimuthal distributions were better fit with Lorentz functions, thus the plot based on equation (5) (as shown in Fig. 6) was used to determine $\langle L_{shish} \rangle$ and $B_{\emptyset}$.

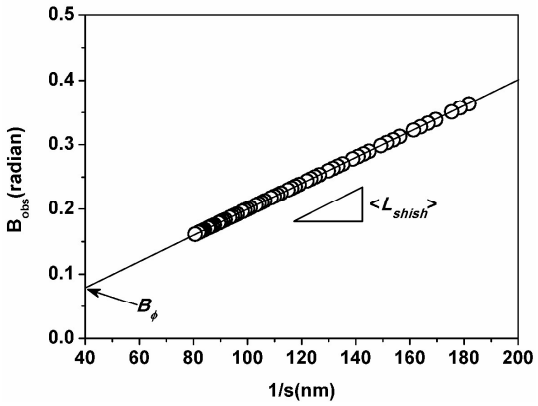


**Fig. 6** Plot of azimuthal integral width ($B_{obs}$) vs the value of $1/s$, which was used to determine the average shish length ($\langle L_{shish} \rangle$) and the shish misorientation ( $B_{\emptyset}$) based on equation (5).

Fig. 7 shows the one-dimensional SAXS scattering intensity distribution curves along $q_1$ direction of UHMWPE gel fibers hot-drawing at different temperature and $DR_1$. The scattering intensity firstly increases and then decreases with the increase of $DR_1$ at 124, 127.5, 130 and 140 °C, which corresponds to the result of kebab scattering intensity. Moreover, the peak position, $q_{1,max}$, which decides the value of long period, $L$, firstly increases and then decreases with the increase of $DR_1$ at 124, 130 and 140 °C. But when the temperature at 127.5 °C, $q_{1,max}$ firstly decreases then increases and finally decreases with the increase of $DR_1$. The information from Fig. 7 is relatively apparent, so the more information about the kebab structure needs to obtain from the value of long period, $L$.

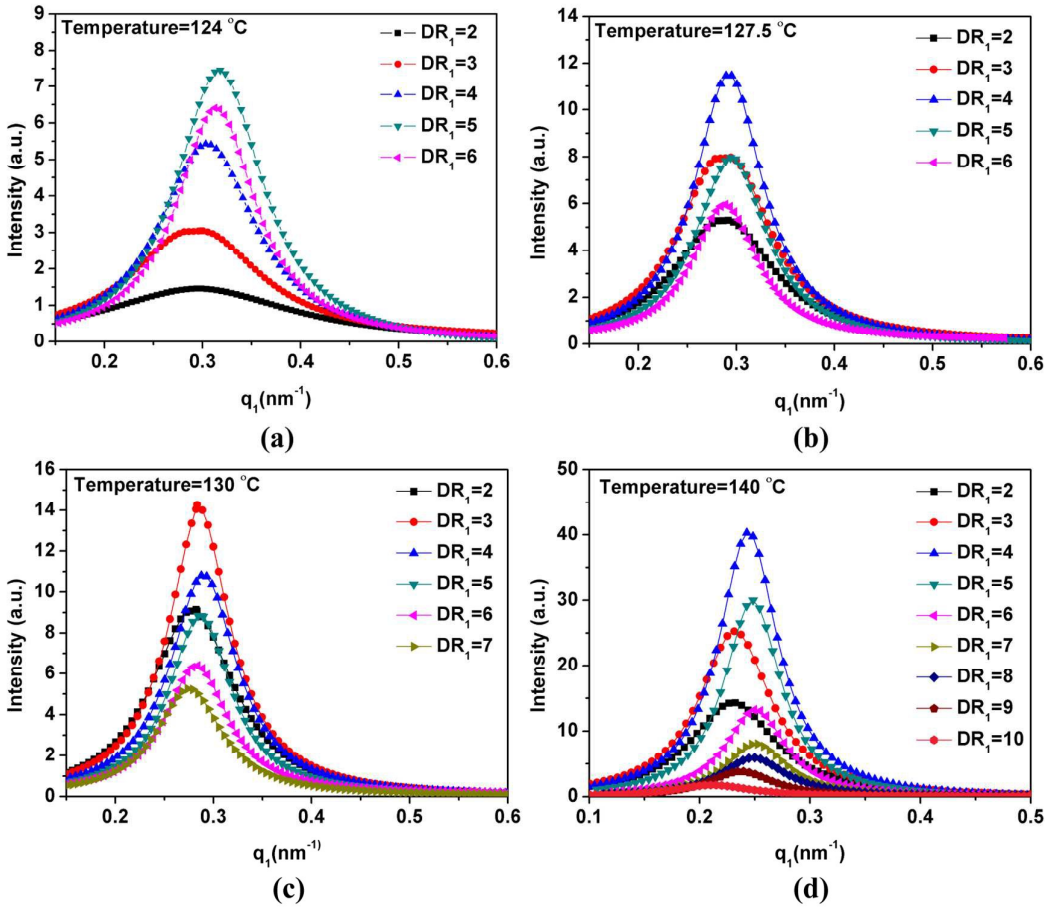


**Fig. 7** One-dimensional SAXS scattering intensity distribution curves along $q_1$ direction of UHMWPE gel fibers hot-drawing at different temperature and $DR_1$.

The long period and the distribution of long period of UHMWPE gel fibers hot-drawing at different temperature and $DR_1$ are shown in Fig. 8. The long period is increased with the temperature and the distribution of long period decreases with the increase of temperature, which is attributed to the decrease of the number of kebab with the increase of temperature due to the fact that the nucleation ability of kebab on shish became weaker with the increase of temperature. But kebab structure is more perfect and bigger with the increase of temperature because that

high temperature is good to the growth of kebab crystals. In addition, the long period at hot-drawing temperature of 124, 130 and 140 °C firstly decrease and then increase, but long period at 127.5 °C firstly increases slightly then decreases and finally increases. The first slight increase at hot-drawing temperature of 127.5 °C should be caused by calculation deviation. So the basic trend of long period is firstly decreased at relative low $DR_1$ and then increased at relative high $DR_1$, which corresponds to the results of kebab intensity. It can be known from Fig. 8 (b) that the distribution of long period at 124, 127.5, 130 and 140 °C decreases with the increase of $DR_1$, which means the long period become more homogeneous with the increase of $DR_1$. Moreover, the main structural process of hot-drawing is the formation of kebab at relative low $DR_1$, while the transformation of kebab to shish occupies the main process of hot-drawing process at relative high $DR_1$. Combining the result of kebab scattering intensity as shown in Fig. 4(b), the decrease of long period at relative low $DR_1$ was attributed to the formation of more kebabs. And the increase of long period at relative high $DR_1$ was caused by the transformation of kebab to shish, which indicates that more kebab transformed to shish with the increase of $DR_1$.

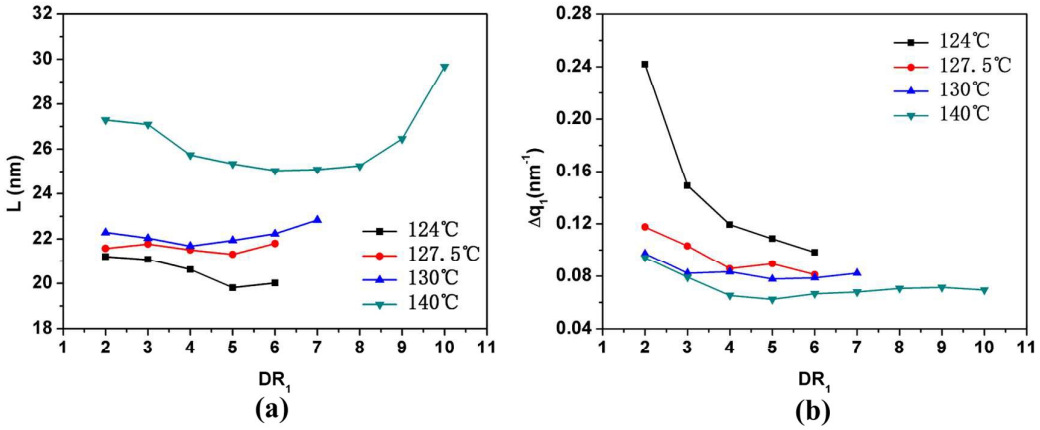


**Fig. 8** (a) The long period of UHMWPE gel fibers hot-drawing at different temperature and $DR_1$, (b) the distribution of long period of UHMWPE gel fibers hot-drawing at different temperature and $DR_1$.

Fig. 9 shows the one-dimensional SAXS scattering intensity distribution curves along $q_2$ direction of UHMWPE gel fibers hot-drawing at different temperature and $DR_1$. The variations of intensity with the increase of $DR_1$ at different temperatures are same as those of Fig. 7. The lateral size of kebab structure of UHMWPE gel fibers hot-drawing at different temperature and $DR_1$ is shown in Fig. 10. It can be seen that the kebab lateral size is increased with the temperature. The result implies that higher temperature is good to the formation of kebab with bigger lateral size. Besides, the kebab lateral size firstly increases and then decreases with the increase of $DR_1$. The increase of kebab lateral size indicates that low $DR_1$ at hot-drawing process is conducive to the formation of kebab with bigger lateral size. Moreover, the increase of kebab lateral size seems to accord with the result of kebab scattering intensity as shown in Fig. 4. The decrease of kebab lateral size was caused by the transformation

of kebab to shish and the formation of kebab with smaller lateral size at relative high $DR_1$. The decrease of kebab lateral size at later hot-drawing process corresponds to the previous study results[19, 31-32].

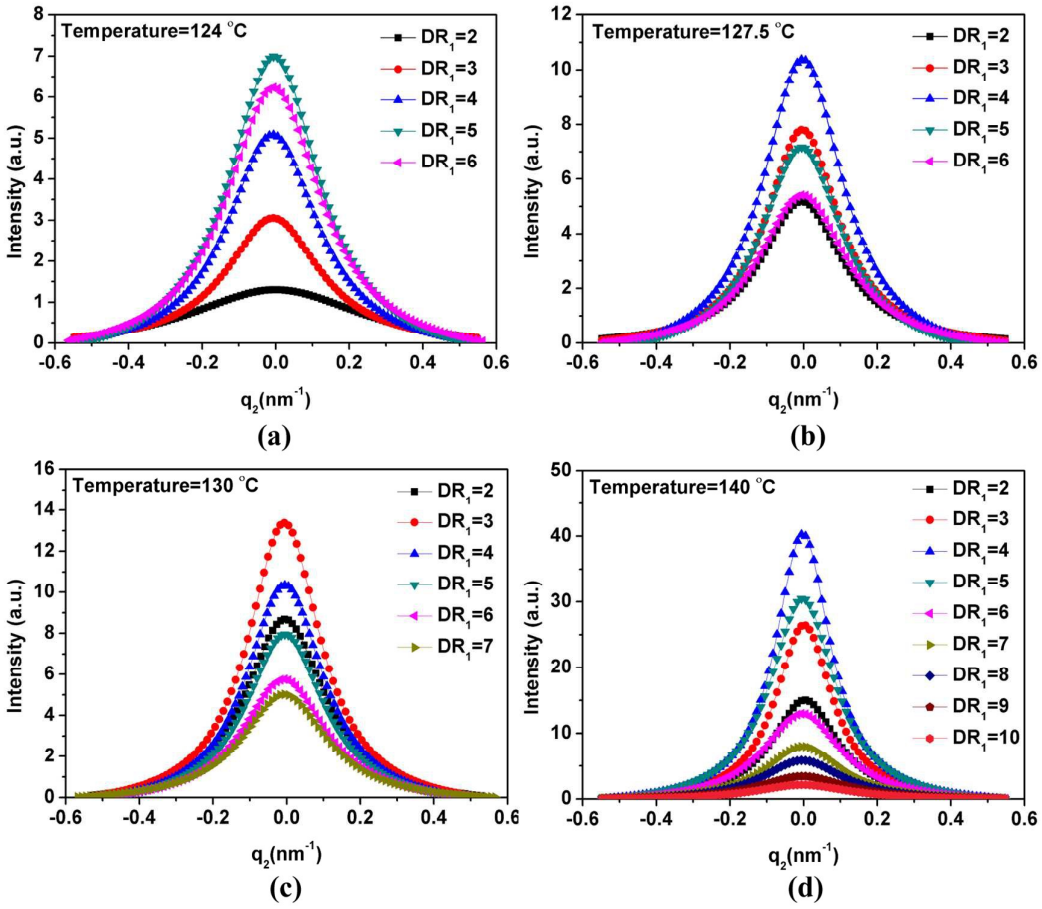


**Fig. 9** One-dimensional SAXS scattering intensity distribution curves along $q_2$ direction of UHMWPE gel fibers hot-drawing at different temperature and $DR_1$.

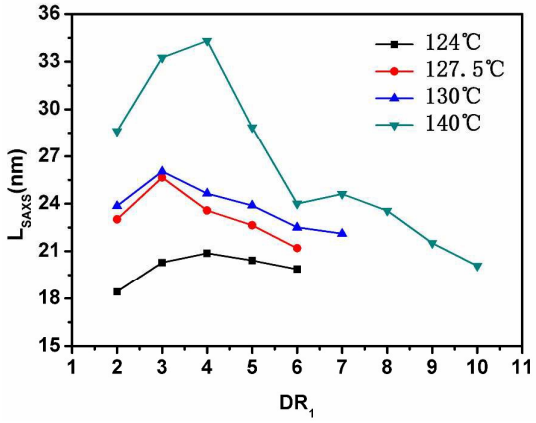


**Fig. 10** The lateral size of kebab structure of UHMWPE gel fibers hot-drawing at different temperature and $DR_1$.

The average shish length ($\langle L_{shish} \rangle$) and the shish misorientation ( $B_{\emptyset}$) of UHMWPE gel fibers hot-drawing at different temperature and $DR_1$ are shown in Fig. 11. It can be easily seen from Fig. 11 (a) that the average shish length at all hot-drawing temperature decreases with the increase of $DR_1$. The decrease of shish length was attributed to the entanglement, which made the shish difficult to growth longer at later stage of hot-drawing process. Moreover, the shish misorientation is also decreased with the increase of $DR_1$ at all hot-drawing temperature, which is due to that hot-drawing at higher $DR_1$ make more shish oriented. With the variation of temperature, no obvious variation trend about average shish length and shish misorientation can be obtained from Fig. 11, which indicates that the hot-drawing temperature has no significant influence on shish length and misorientation.

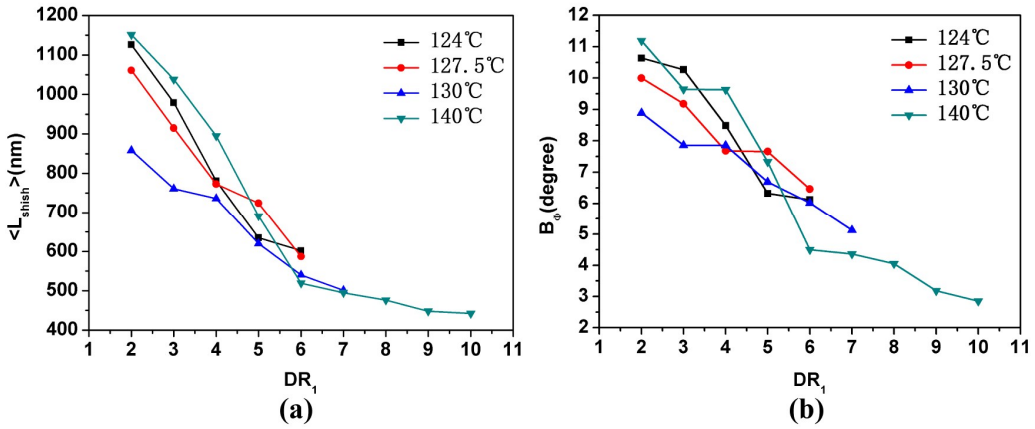


**Fig. 11** (a) The average shish length ($\langle L_{shish} \rangle$) of UHMWPE gel fibers hot-drawing at different temperature and $DR_1$, (b) the shish misorientation ($B_{\emptyset}$) of UHMWPE gel fibers hot-drawing at different temperature and $DR_1$.

On the basis of the previous experimental results and analysis, a schematic diagram is proposed to describe the microstructural evolution of UHMWPE gel fibers during one-step hot-drawing, as shown in Figure 11. Before the hot-drawing process, the lamellae in UHMWPE gel fibers are randomly oriented as shown in Fig. 12 (a). When the hot-drawing process with low $DR_1$ is carried out, the original lamellae transforms to the new shish-kebab cryatals with good orientation as shown in Fig. 12 (b). With the $DR_1$ further to increase, the kebab gradually transforms to microfibril (imperfect shish) structure and the shish length gradually decreases. Finally, not all kebabs transform to microfibril due to the break of the fibers at high $DR_1$ as shown in Fig. 12(c), which indicates that the further transformation of kebab needs next step hot-drawing at higher temperature before the fibers breaking at first-step hot-drawing process.

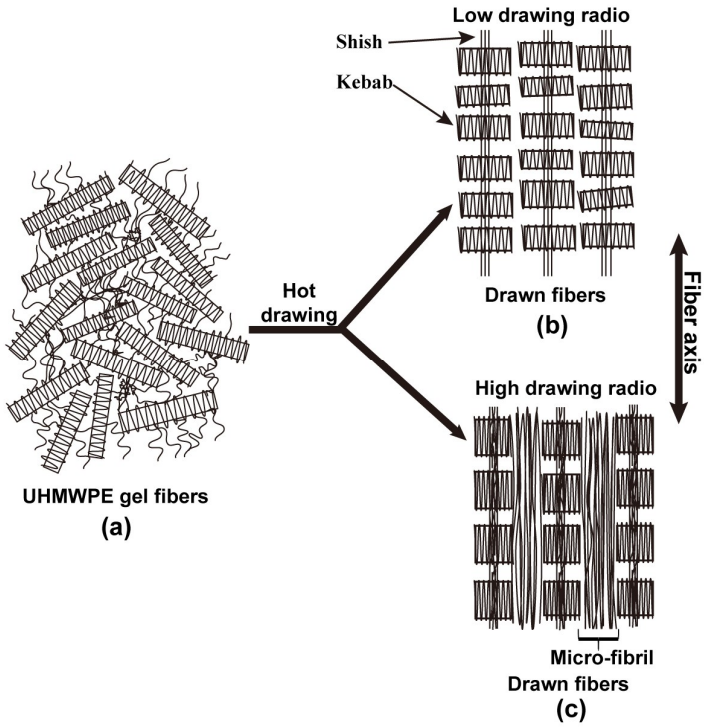


**Fig. 12** Schematic diagram of the microstructural evolution of UHMWPE gel fibers in one-step hot-drawing process.

## 4 Conclusions

The in situ SAXS with the equipment of simulating the hot-drawing process in industrial product line was used to study the structural effects of temperature and drawing ratio ($DR_1$) of hot-drawing process on UHMWPE gel fibers. The increase of temperature is conducive to the formation of less and bigger kebab but no effect on the shish length and misorientation except its quantity. The kebab lateral size increases with the increase of hot-drawing temperature. Moreover, the increase of temperature is beneficial to the formation of shish at relative low temperature range, while the formation of shish at high temperature needs higher $DR_1$. The increase of

$DR_1$ is good to the formation of shish at hot-drawing of all experimental temperatures, while the kebab formation mainly occurred at low $DR_1$ and the kebab transformation mainly happened at high $DR_1$. The increase of $DR_1$ decreases shish length and misorientation. This study has an important significance on further improving the mechanical performance of UHMWPE fibers in industrial product line.

**Acknowledgments**

This work was supported by the National Science Foundation of China (51273210), Open Research Fund of State Key Laboratory of Polymer Physics and Chemistry, Changchun Institute of Applied Chemistry, Chinese Academy of Sciences and K. C. Wong Magna Fund in Ningbo University. We thank Shanghai Synchrotron Radiation Facility (SSRF) for supporting the WAXD and SAXS tests.

**References**

1. D. C. Prevorsek, H. B. Chin and A. Bhatnagar, *Compos Struct,* 1993, **23**, 137-48.

2. R. S. Porter, T. Kanamoto and A. E. Zachariades, *Polymer*, 1994, **35**, 4979-4984.

3. S. Kavesh and D. C. Prevorsek, *International Journal of Polymeric Materials*, 1995, **30**, 15-56.

4. N. D. Jordan, R. H. Olley, D. C. Bassetta, P. J. Hineb and I. M. Ward, *Polymer*, 2002, **43**, 3397-3404.

5. S. R. Dyer, L. V. J. Lassila, M. Jokinenben and P. K. Vallittu, *Dental Materials*, 2004, **20**, 947-955.

6. R. Marissen, *Materials Sciences and Applications*, 2011, **2**, 319-330.

7. M. An, H. Xu, Y. Lv, T. Duan, F. Tian, L. Hong, Q. Gu, and Z. Wang, *RSC Advances*, 2016, **6**, 20629-20636.

8. J. Smook, W. Hamersma and A. J. Pennings, *Journal of materials science*, 1984, **19**, 1359-1373.

9. A. J. Pennings and J. Smook, *Journal of materials science,* 1984, **19**, 3443-3450.

10. W. Hoogsteen, A. J. Pennings and G. Tenbrinke, *Colloid and Polymer Science,* 1990, **268**, 245-255.

11. Y. Ohta, H. Murase and T. Hashimoto, *Journal of Polymer Science Part B: Polymer Physics,* 2005, **43**, 2639-2652.

12. J. T. Yeh, S. C. Lin, C. W. Tu, K. H. Hsie and F. C. Chang, *Journal of Materials Science*, 2008, **43**, 4892-4900.

13. V. M. Litvinov, J. J. Xu, C. Melian, D. E. Demco, M. Moller and J. Simmelink, *Macromolecules,* 2011, **44**, 9254-9266.

14. D. Krueger, and G. S. Y. Yeh, *Journal of Macromolecular Science Part B: Physics*, 1972, **6**, 431-450.

15. J. Smook and A. J. Pennings, *Journal of Applied Polymer Science*, 1982, **27**, 2209-2228.

16. M. Xiao, J. Yu, J. Zhu, L. Chen, J. Zhu, and Z. Hu, *Journal of materials science*, 2011, **46**, 5690-5697.

17. H.G. Chae and S. Kumar, *Science*, 2008, **319**, 908-909.

18. Y. Tian, C. Zhu, J. Gong, S. Yang, J. Ma, and J. Xu, *Polymer*, 2014, **55**, 4299-4306.

19. Y. Tian, C. Zhu, J. Gong, J. Ma, and J. Xu, *European Polymer Journal*, 2015, **73**, 127-136.

20. J. Rathje and W. Ruland, *Colloid and Polymer Science*, 1976, **254**, 358-370.

21. X. D. Liu and W. Ruland, *Macromolecules*, 1993, **26**, 3030-3036.

22. A. F. Thünemann and W. Ruland, *Macromolecules*, 2000, **33**, 1848-1852.

23. M. F. Butler, A. M. Donald, W. Bras, G. R. Mant, G. E. Derbyshire and A. J. Ryan, *Macromolecules*, 1995, **28**, 6383-6393.

24. F. Tian, X. H. Li, Y. Z. Wang, C. M. Yang, P. Zhou, J. Y. Lin, J. R. Zeng, C. X. Hong, W. Q. Hua, X. Y. Li, X. R. Miao, F. G. Bian and J. Wang, *Nuclear Science and Techniques*, 2015, **26,** 1-6.

25. A. P. Hammersley, S. O. Svensson and A. Thompson, *Nuclear Instruments and Methods in Physics Research*, 1994, **346**, 312-321.

26. J. K. Keum, F. Zuo and B. S. Hsiao, *Macromolecules*, 2008, **41**, 4766-4776.

27. Y. Tang, Z. Jiang, Y. Men, L. An, H. F. Enderle, D. Lilge and J. Rieger, *Polymer*, 2007, **48**, 5125-5132.

28. W. Ruland, *Journal of Polymer Science Part C: Polymer Symposia*, 1969, **28**, 143-151.

29. W. Ruland and R. Perret, *Journal of Applied Crystallography*, 1969, **2**, 209-218.

30. W. Ruland and R. Perret, *Journal of Applied Crystallography*, 1970, **3**, 525-532.

31. Y. Ohta, H. Murase and T. Hashimoto, *Journal of Polymer Science: Part B: Polymer Physics*, 2010, **48**, 1861-1872.

32. H. Liu, F. Lv, J. Li, T. Cao, C. Wan, W. Zhang, L. Li, G. Zheng and C. Shen, *Journal of*

*Applied Polymer Science*, 2015, **132**, 42823- 42833.